Theoretical Insights to Niobium-Doped Monolayer MoS_2–Gold Contact

Anuja Chanana and Santanu Mahapatra, *Senior Member, IEEE*

***Abstract*— We report a first principles study of the electronic properties for a contact formed between Nb-doped monolayer MoS_2 and gold for different doping concentrations. We first focus on the shift of energy levels in band structure and the density of states with respect to the Fermi level for a geometrically optimized 5 × 5 MoS_2 supercell for both pristine and Nb-doped structures. The doping is achieved by substituting Mo atoms with Nb atoms at random positions. It is observed that for an experimentally reported sheet hole doping concentration of (ρ_{2D}) 1.8×10^{14} cm^{-2}, the pristine MoS_2 converts to degenerate p-type semiconductor. Next, we interface this supercell with six layers of ⟨111⟩ cleaved surface of gold to investigate the contact nature of MoS_2–Au system. By careful examination of projected band structure, projected density of states, effective potential and charge density difference, we demonstrate that the Schottky barrier nature observed for pure MoS_2–Au contact can be converted from n-type to p-type by efficient Nb doping.**

***Index Terms*— Density functional theory (DFT), doping, MoS_2, niobium, Schottky barrier height (SBH).**

I. Introduction

COVALENTLY bonded monolayer MoS_2 is a potential channel material for future ultrathin body MOSFET [1]. MoS_2 crystals are shown to have n-type, nature mostly in experimentally reported transistors [2]–[6]. However, for the successful realization of CMOS circuitry, high-performance p-channel MoS_2 transistor is equally required. It is challenging to find a suitable atom for MoS_2 crystal which is competent enough to donate holes and be thermodynamically stable at the same time. Using the first principles analysis, niobium emerged as a possible choice among all the p-type dopants for Mo [7]. A p-channel transistor making use of p-type MoS_2 crystals fabricated using chemical vapor transport [8] and chemical vapor deposition [9] is attained successfully. The p-type nanoparticles made of Nb-doped MoS_2 are also synthesized [10]. Since the nature of MoS_2–metal contacts significantly affects the functioning of transistor, it is of utmost importance to probe into the theoretical insights of the electronic properties of Nb-doped MoS_2–metal contact apart from the experiments [8].

Manuscript received March 16, 2015; revised May 7, 2015; accepted May 13, 2015. Date of publication June 2, 2015; date of current version June 17, 2015. The work was supported by the Science Engineering and Research Board–Department of Science and Technology, Government of India, under Grant SR/S3/EECE/0151/2012. The review of this paper was arranged by Editor A. Haque.

The authors are with the Nano-Scale Device Research Laboratory, Department of Electronic Systems Engineering, Indian Institute of Science, Bangalore 560012, India (e-mail: anuja@cedt.iisc.ernet.in; santanu@dese.iisc.ernet.in).

Color versions of one or more of the figures in this paper are available online at http://ieeexplore.ieee.org.

Digital Object Identifier 10.1109/TED.2015.2433931

In this paper, we investigate the contact nature in an interface formed by pure and Nb-doped MoS_2 supercell with Au (most commonly used in experiments) by employing density functional theory (DFT). We first examine the electronic properties of pure and Nb-doped structures in a 5 × 5 supercell of MoS_2. The doping concentration is varied from 4×10^{13} to 1.8×10^{14} cm^{-2}, and the total number of dopants replacing Mo atoms is calculated using the formula $\rho_{2D}\times$(area of hexagonal sheet) respective to each doping concentration value. We consider five different structures where Nb is substituted by Mo at random positions and using the formation energy calculations (E_{form}), the most stable structure is determined. It is observed that the n-type MoS_2 shows a transformation to p-type with valence band (VB) shifting toward the Fermi level (E_F) and for high values of doping concentration, the VB even crosses the E_F, thus making MoS_2 a degenerate p-type semiconductor. Furthermore, we make an interface of this optimized supercell with ⟨111⟩ cleaved surface of Au and explore the contact nature of this system. To calculate the Schottky barrier height (SBH) for these interfaces, we make use of band structure and projected density of states (PDOS), and relative shifts in the VB and conduction band (CB) with respect to E_F are explained by an effective potential analysis. Charge redistribution and orbital hybridization are studied using charge density difference analysis and PDOS. Based on all the above analysis, we eventually conclude that doping achieved by effective substitutional atoms is successful in acquiring p-type conduction in MoS_2, and can be utilized further to reduce the MoS_2–metal contact resistances.

II. Computational Details

Our DFT calculations (based on conventional Kohn–Sham Hamiltonian [11], [12]) utilize generalized gradient approximation (GGA) with Perdew–Burke–Ernzerhof form [13], [14] of the exchange-correlation functional, as implemented in Atomistix Tool Kit [15]. Since GGA is well known to underestimate the bandgap of MoS_2 [16], we first investigate the bandgap of monolayer MoS_2 (lattice constant = 3.1604 Å). Pseudopotentials of molybdenum (Mo) and sulfur (S) generated using the Hartwingster–Goedecker–Hutter [17] scheme with Tier 4 basis set are found to give accurate bandgap of 1.8 eV, which is consistent with the experimental results [18]. We continued with the same pseudopotential and Tier set for niobium and gold in order to maintain consistency in accuracy in this paper. The iteration control parameters consist of Pulay mixer algorithm using 100 as a maximum number of iteration steps and 10^{-5} Hartree as the tolerance value.

0018-9383 © 2015 IEEE. Personal use is permitted, but republication/redistribution requires IEEE permission.
See http://www.ieee.org/publications_standards/publications/rights/index.html for more information.

The Brillouin zone is sampled by 9 × 9 × 1 Monkhorst–Pack k meshes [19] using a density mesh cutoff of 75 Hartree. All the simulations are done using the aforementioned functional and parameters.

A 5×5 hexagonal supercell of MoS_2 with lateral dimensions of 15.802 × 15.802 Å^2, as reported earlier in [7], is found appropriate to study the effect of doping by substitutional atoms. Moreover, for MoS_2–Au interface, this supercell size is computationally acceptable, as the interface strain found is 1.1%, and it further increases from 4% to 36% for supercell sizes ranging from 6 × 6 to 10 × 10. Experimentally reported value of high sheet hole concentration ρ_{2D} 1.8×10^{14} cm^{-2} [8] corresponds to a total of 4.5 dopants in this supercell. Accordingly, in this paper, we investigate 0–4 Nb dopants in a 5 × 5 MoS_2 supercell. To maintain the comprehensiveness in this paper, we do the interface study only for 0, 2, and 4 Nb doping cases. The pure and Nb substituted MoS_2 supercell and unit cell of gold and niobium in bulk fcc phase are relaxed using limited memory Broyden–Fletcher–Goldfarb–Shannon method [20] until the forces on the atom are 0.05 eV/Å. This optimized supercell is interfaced with six layers of ⟨111⟩ cleaved surface of gold. A vacuum region of more than 20 Å is kept normal to the MoS_2–Au interface structure to suppress the effects of artificial and spurious interactions between the individual structures.

III. Results and Discussion

A. Nb-Doped MoS_2 Supercell and Interface Contact Geometry

Amongst all the feasible p-type dopants (having electrons less than Mo in d-orbital) at the Mo-position, niobium is found to be the most promising candidate [7]. To ensure the stability of substitutional doping in MoS_2 supercell, we calculate the (E_{form}) for each supercell given by the following equation [21]:

$$E_{\text{form}} = E_{\text{total}}(MoS_2 + Nb) - E_{\text{total}}(MoS_2) + n(\mu_{\text{Mo}}) - m(\mu_{\text{Nb}}) \quad (1)$$

where $E_{\text{total}}(MoS_2 + Nb)$ is the total energy of the Nb substituted MoS_2 supercell in electronvolt, $E_{\text{total}}(MoS_2)$ is the total energy of pristine MoS_2 supercell in electronvolt, μ_{Mo} and μ_{Nb} are the chemical potentials of individual Mo and Nb atoms in bulk FCC phases with the units of electronvolt, and n and m denote the number of Mo and Nb atoms, respectively. We simulate five structures for each number of dopants ranging from 1 to 4, where the number of Nb dopants is randomly distributed in the MoS_2 supercell and choose the supercell with minimum E_{form}. Then, we interface this structure with six layers of ⟨111⟩ cleaved Au surface only for 0, 2, and 4-Nb-doped supercells. Fig. 1(a) shows the most stable hexagonal geometry of MoS_2 supercell with randomly dispersed 4 Nb dopants. While interfacing each thermodynamically stable Nb-doped MoS_2 supercell, with Au, we observe that the strain value remains 1.1%.

To find the most stable geometry of MoS_2–Au interface, we perform binding energy (BE) calculations with varying interlayer distances between the two structures. Table I depicts the values of E_{form}, BE, and interlayer separation

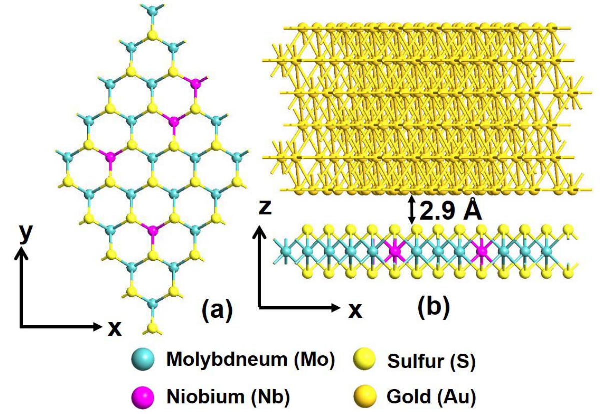

Fig. 1. (a) Optimized geometry of 4-Nb-doped MoS_2 supercell. Niobium is doped randomly all over the supercell. (b) Interface geometry of 4-Nb-doped MoS_2 with six layers of ⟨111⟩ cleaved gold surface and the interlayer distance corresponding to minimum BE.

TABLE I
BINDING AND FORMATION ENERGIES FOR PURE AND NIOBIUM SUBSTITUTED MoS_2 SUPERCELLS

Number of dopants	E_{form}(eV)	BE(eV)	Equilibrium Distance
0	–	-3.57	3.1Å
2	-0.382	-5.339	3.1Å
4	-0.78	-6.103	2.9Å

between MoS_2-Au with increasing the number of dopants. Notably, the value of E_{form} becomes more negative by increasing the number of dopants, which means that presumably the Nb substitution is stable under thermodynamic conditions. The interlayer distance decreases when the number of dopants increase which implies there must be a better charge redistribution at the interface, which results in a significant modification of SBH at the interface. Fig. 1(b) shows the interface contact geometry of 4-Nb-doped MoS_2 supercell with gold, having an equilibrium interlayer distance of 2.9 Å in a hexagonal lattice structure. This distance is less than the distance obtained for pure MoS_2–Au interface and even MoS_2 (2-Nb doped)–Au, and it is expected that the SBH will be less for 4-Nb-doped MoS_2 supercell in comparison with 2-Nb-doped interface geometry.

B. Band Structure and DOS of Pure and Doped MoS_2 Supercell

Before proceeding into the evaluation of MoS_2–Au contact nature, we develop insights to the electronic properties of pure and doped MoS_2 supercells. We simulate MoS_2 supercell with increasing the number of dopants from 1 to 4 by replacing Mo atoms with Nb atoms. Fig. 2 shows the band structure (left-hand side) and DOS (right-hand side) of pure and doped 5 × 5 MoS_2 supercell with a proper alignment of E_F. Here, we observe that for a doped MoS_2 supercell, the VB shifts upward with respect to Fermi level at the proximity of E_F as compared with pure supercell. With the increase in doping, the shift is even more pronounced and it even crosses the E_F, which shows this amount of doping is actually a degenerate

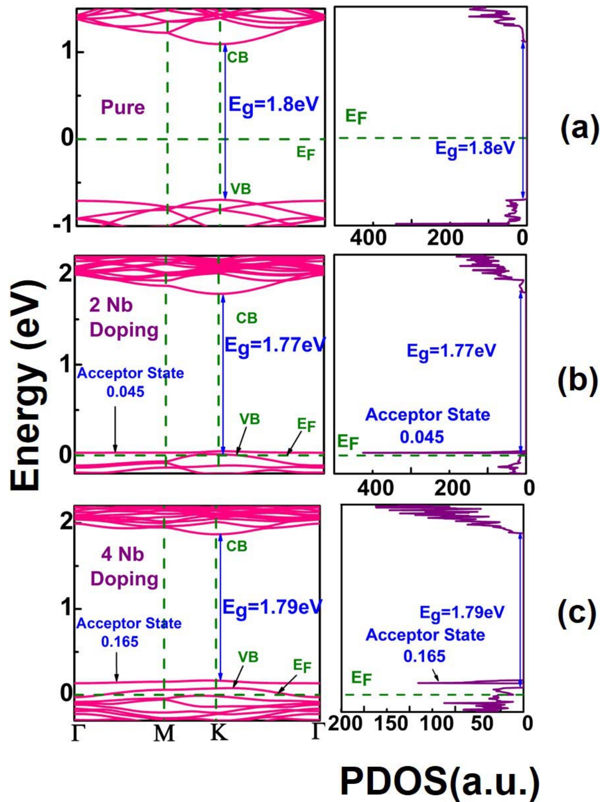

Fig. 2. Band structure and PDOS for optimized structures of (a) pure MoS_2, (b) 2-Nb-doped MoS_2, and (c) 4-Nb-doped MoS_2. Acceptor states are formed for both 2 and 4 Nb doping in (b) and (c), and it is higher for a large number of dopants, i.e., 4. Bandgap varies for the doped structure due to a variation in the Mo–S bond length and the emergence of Nb–S bonds due to Nb doping. CB, VB, E_F, and E_g denote CB edge, VB edge, Fermi level, and bandgap, respectively.

doping for MoS_2 supercell. There is also an acceptor state formation for doped supercells and it is at a higher level with the increase in the number of dopants. As the amount of doping is increased to 4, we observe that the acceptor state is formed at 0.165 eV as compared with 0.045 for 2-Nb-doped supercell, evident from Fig. 2(b) and (c). One more interesting point noticed here is a minor variation in the bandgap of MoS_2 supercell. For pure MoS_2 supercell, the bandgap value obtained exactly is 1.8 eV. However, with Nb doping, the bandgap varies, which can be attributed to the change in the bond length of Mo–S and the emergence of a new Nb–S bond with Nb substitution. However, the value is more closer to the exact with 4 Nb doping. It is observed that the average bond length of the pristine MoS_2 supercell does not significantly change even after replacing 4 Mo atoms with Nb. Thus, the bandgap remains unchanged with doping. However, at the same time, even with a single Mo atom replacement with Nb an acceptor state close to the VB is created leading to a significant shift of VB maxima (VBM).

Table II depicts the values of both CB minima (CBM) and VBM for doped MoS_2 supercell with the increasing number of dopants from 1 to 4. It is observed here that with the increase in the number of dopants, the value of CBM becomes more positive, VBM shows a negative-to-positive transition, and the acceptor state too becomes more positive. If we compare

TABLE II
CBM AND VBM FOR PURE AND NIOBIUM SUBSTITUTED MoS_2 SUPERCELLS

Number of dopants	CBM(eV)	VBM(eV)	Acceptor State(eV)
0	1.09	-0.67	–
1	1.75	-0.014	-0.0071
2	1.78	0.012	0.045
3	1.83	0.027	0.15
4	1.87	0.075	0.165

Mo([Kr] $4d^5$ $5s^1$) and Nb([Kr] $4d^4$ $5s^1$) in their electronic configurations, we see that Nb is deprived of one electron in the d-orbital, which makes it positive as compared with Mo atom. Therefore, we can see an acceptor state and an increase in its value with an increase in Nb dopants (due to the decrease in the number of electrons).

C. MoS_2–Au Contact Evaluation (Pure and Nb Doped)

We continue by performing DFT simulations to develop comprehensive concepts regarding the MoS_2—Au (pure and Nb doped) contact evaluation. We present a detailed analysis of band structure, density of states, charge density difference, and effective potential to understand the nature of contact formation for pure and Nb-doped MoS_2 supercells. The main observation is the variation of SBH at the MoS_2–metal interface calculated using band structure and DOS. The relative shifts in energy levels and charge redistribution is further explained using effective potential and charge density difference.

1) Schottky Barrier Height Evaluation Using Band Structure and Density of States: To evaluate the nature of contact (Schottky or Ohmic) of the MoS_2 (pure and doped)–Au interface, we perform band structure and DOS calculations (projected MoS_2), as shown in Fig. 3. For a combined MoS_2–Au systems, due to strong interface orbital hybridization, it is difficult to identify the MoS_2 CB and VB [22], and it becomes more difficult with doping. This complication arises because of Nb substitution, Mo–S bond length varies and Nb–S bond appears, which alter the bands to a high degree, but still they are recognizable to some extent. Before depicting details regarding the Schottky barrier, we closely examine both VB and CB with a perfect alignment of E_F of projected MoS_2, keeping aside band structure and DOS, as shown in Fig. 3. For pure MoS_2 [Fig. 3(a)], the CB and VB are clearly visible and the bandgap is confirmed by DOS with minimum or no mid gap states. For 2 Nb doping [Fig. 3(b)], the VB is clearly visible with an acceptor state at -0.585 eV but CB is ambiguous along with a few mid gap states. The CB is identified among all the midgap states, and using DOS, we find that the contribution of these mid gap states is negligible. Thus, we confirm the exact position of CB and VB by measuring the bandgap between two and found it approximately equal to 1.8 eV. Since this is a heterogeneous interface, due to strong interface orbital hybridization, the accurate value of MoS_2 bandgap is difficult to obtain. The absolute positions of CB and VB are shown by connecting them in both DOS and band structure plot, as shown in Fig. 3 (light blue lines). In the case of 4 Nb doping [Fig. 3(c)] as well, the VB is visible

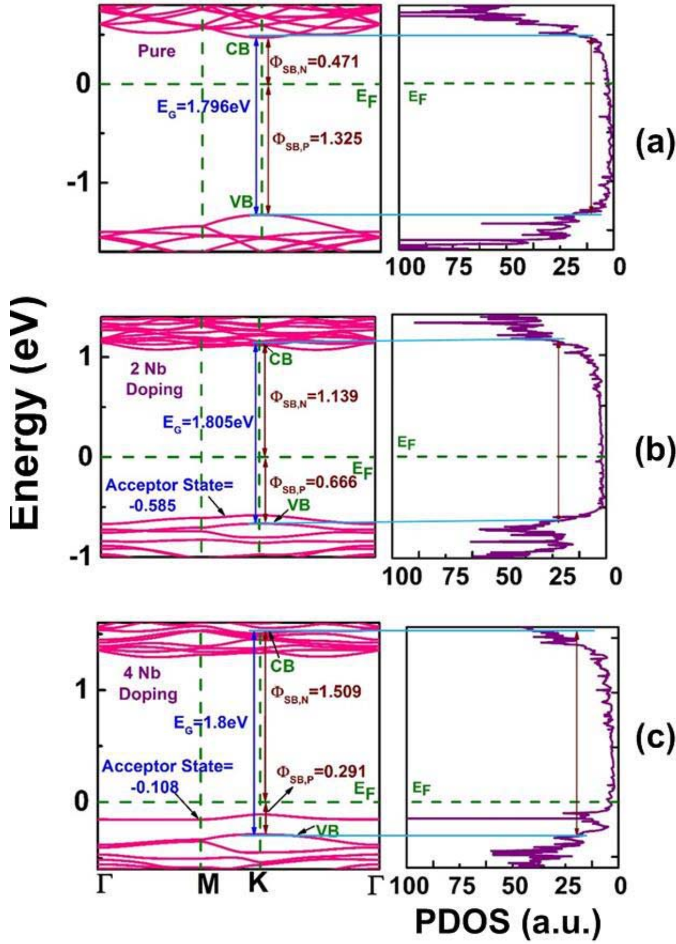

Fig. 3. Projected band structure and DOS of (a) pure, (b) 2-Nb-doped, and (c) 4-Nb-doped MoS_2 supercell for MoS_2–Au interface geometry. CB and VB are the CB and VB edge, respectively. $\phi_{SB,P}$ and $\phi_{SB,N}$ are the p-type and n-type Schottky barriers. E_F and E_g denote Fermi level and bandgap, respectively. Acceptor states are seen for Nb dopants, and it is higher for 4 Nb doping. Fermi levels are aligned to figure the positions of VB and CB edges and are connected by straight blue lines in both band structure and DOS.

and acceptor state is formed at −0.108 eV which is higher than 2 Nb doping. A spike at that particular value is also seen in DOS. We follow the same methodology of observing CB in 4-Nb-doped interface geometry as done for 2 Nb doping.

The value of SBH is calculated as $E_C - E_F$ (n-type) and $E_F - E_V$ (p-type) using the projected band structures of MoS_2. As we can see from Fig. 3(a), pure MoS_2 gives an n-type SBH with a value of 0.471 eV and a p-type SBH of 1.325 eV. Au is found to be an n-type contact for MoS_2 which is consistent with the previous reports [23]. The bandgap of MoS_2 is also quite similar to that of the original value. For 2-Nb and 4-Nb-doped MoS_2, we observe that there is a drastic transition in the type of SBH obtained. Since Nb is a p-type dopant for MoS_2, we see that the n-type barrier increases to 1.139 eV and p-type barrier (0.666 eV) decreases with the formation of acceptor state. The p-type SBH decreases to 0.291 eV and n-type SBH increases to 1.509 eV when the Nb dopants increase to 4. Thus, from the above analysis, we can conclude that a doping concentration corresponding to four number of dopants is successful in significant alteration of p-type SBH at the MoS_2–Au interface.

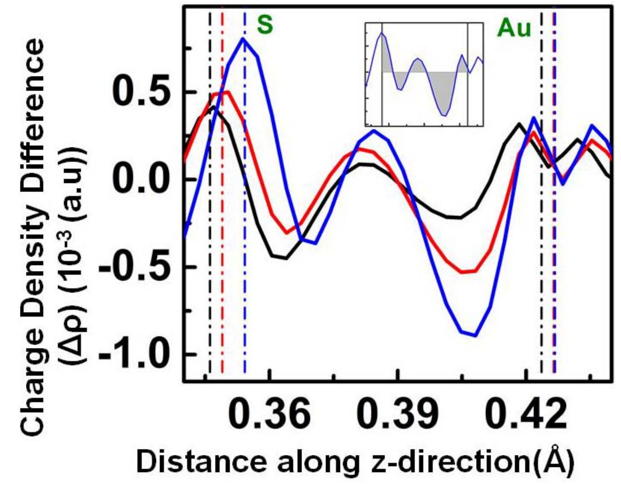

Fig. 4. Average charge density difference versus the fractional distance along the y-direction. The distance is limited only at the interface between the nearest S atom and the nearest gold atom. The respective position of the interfacial atoms is denoted by dashed black, red, and blue lines for pure, 2 and 4 Nb doping, respectively. The position of gold atom shows a near overlap for 2 and 4 Nb doping. Inset: area calculated between the interfacial atoms.

2) Charge Density Difference: To develop further understanding regarding the charge movement across the interface, we calculate the charge difference analysis given by

$$\Delta\rho = \rho_{MoS_2(\text{pure/doped})+\text{Gold}} - \rho_{MoS_2(\text{pure/doped})} - \rho_{\text{Gold}} \quad (2)$$

where $\rho_{MoS_2(\text{pure/doped})+\text{Gold}}$ is the charge density of the complex system, $\rho_{MoS_2(\text{pure/doped})}$ is the charge density of pure/doped MoS_2 supercell, and ρ_{Gold} is the charge density of gold slab [24].

Fig. 4 shows the charge density difference for pure and all the doping interfaces assembled in a single plot. Here, we see a dipole formation showing peaks at both the negative and positive sides at the interface. It leads to another observation that both the charge accumulation and the depletion region exists at the interface, and it increases with an increase in the number of dopants. However, the increase in depletion region is more pronounced as compared with the accumulation. In Fig. 4 (inset), we show the area calculated in the interfacial region formed of the nearest S and the nearest Au atomic layers. When we compare this area for the pure and doped cases, we find that the area is more negative for 4-Nb-doped interface, which means that the depletion regime is higher for 4-Nb-doped system as compared with 2-Nb doped and pure. Hence, for 4-Nb-doped system, the interface is devoid of charge carriers making it more p-type doped [25], thus shifting the VB more toward the E_F. If we analyze the depletion at the gold atom and the accumulation at the sulfur atom for all the three systems, we observe that both the depletion and the accumulation increase with the dopant increase. Therefore, more charge transfer takes place from gold to sulfur side with doping and shows a better barrier reduction for this system. In addition, due to a large accumulation, a strong orbital hybridization occurs at the 4-Nb-doped MoS_2–Au system [26].

We also evaluate average electron density at the interface, which gives a measure of quantum mechanical probability of locating electrons at particular positions in space [27].

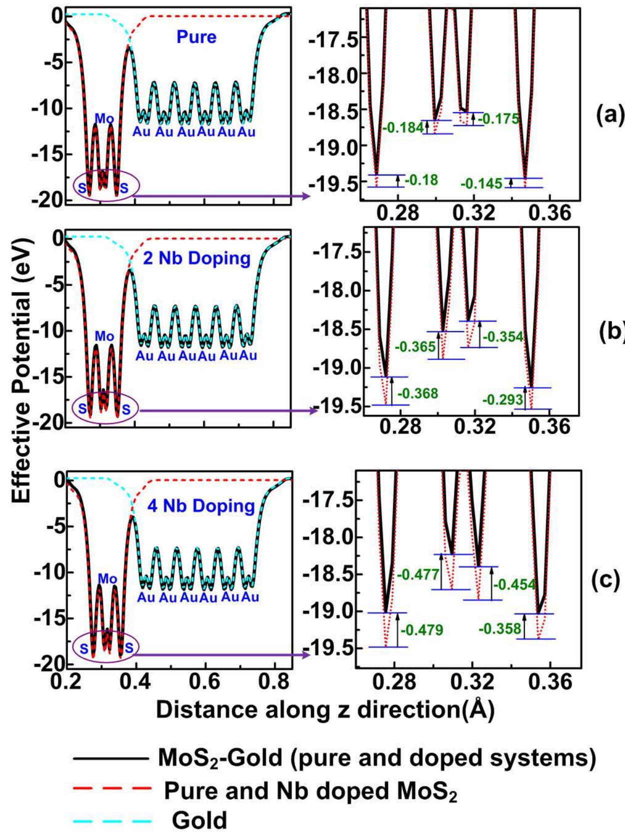

Fig. 5. Effective potential of MoS_2–Au system and only MoS_2 for (a) pure MoS_2, (b) 2-Nb-doped MoS_2, and (c) 4-Nb-doped MoS_2. The potentials of MoS_2 (red dashed lines) and six layers of gold (cyan dashed lines) before forming the interface are aligned with the effective potential of the MoS_2–Au interface. The overlap of pure MoS_2 with the interface structure is elaborated on the right-hand side for all the three systems.

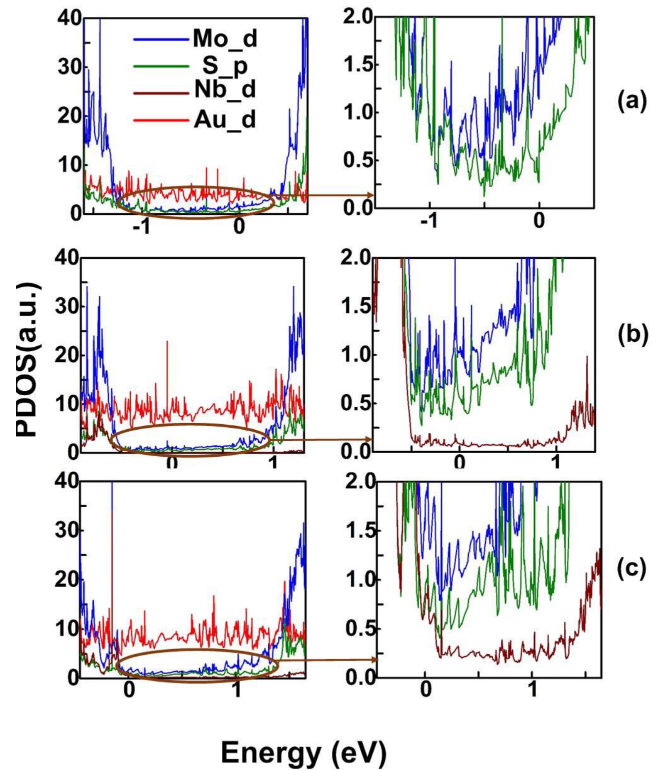

Fig. 6. PDOS showing the individual orbital contribution of interfacial atoms (the nearest layer of S atoms and Au atoms) and Mo atoms with dopant Nb for (a) pure, (b) 2-Nb-doped, and (c) 4-Nb-doped supercell. The major contribution comes from the d-orbitals of Mo and Nb, d-orbitals of Au, and p-orbitals of S in all cases. Since the number of Nb atoms is much less than Mo, S, and Au atoms; its contribution is also quite small. Plots on the right-hand side elaborate the contribution of orbitals of Mo, Nb, and S atoms, highlighted by brown ring in the left-hand side figure.

Higher values indicate a better feasibility of charge transfer. The values of electron density are found to be 0.083(4 Nb), 0.0607(2 Nb), and 0.0606(pure) $Å^{-3}$. The highest value is obtained for 4-Nb-doped interface, which facilitates easy transfer of charge carrier across this interface.

3) Effective Potential: Fig. 5 shows the effective potential of pure and doped MoS_2–Au geometry with the effective potential of individual MoS_2 (dashed red lines) and six layers of gold (dashed cyan lines) superimposed that are obtained before the formation of interface. The shifts observed in individual gold slab are <0.1 eV while for individual MoS_2 considerable shifts in the potential are observed. The effective potential of MoS_2 is expanded to highlight these changes with respect to the doping as shown on the right-handside for each interface pointed by violet arrows. Here, it is found that there is a shift in the potentials for pure MoS_2, which can be attributed to the interaction of MoS_2 with gold similar to the effect observed in [25] for graphene–metal contacts. While comparing the variation of pure and doped interface, we see that it increases with the increase in doping, which implies a better interaction between the doped supercell and the gold slab. The change is almost double for 2-Nb-doped interface in comparison with the pure interface, and it further enhances for 4-Nb-doped case implying a stronger interaction. Moreover, there is an upward shift in the potentials, which is consistent with the shifts observed in the energy levels in band structure and DOS for pure and doped supercells as explained earlier. Therefore, from the above observations, we confirm the nature of shift in energy levels is upward, and both the shifts and the charge interaction are maximum for 4-Nb-doped interface.

4) Orbital Hybridization Using Projected Density of States: In the section Charge Density Difference, while discussing about the formation of accumulation region at the MoS_2–metal interface, we highlight the point that it increases with enhancement in doping. By a careful scrutiny of the individual orbital contribution, it is found out that this accumulation region is attributed to the strong MoS_2–Au hybridization. It is well known that the contribution of Mo–d orbitals is greater than S–p orbitals and the same can be seen from Fig. 6. If observed carefully, we see a strong correspondence among all the orbital contribution as there is a similarity in the nature of states. In the bandgap regime, the PDOS has low values, so we highlight the contributions in the right-hand side of each figure and observe that the PDOS of various orbitals are similar to each other. For Nb, we observe that when the number of dopants increase from 2 to 4 the corresponding states rise high and effectively tends to decrease the nearly equivalent zero states in the bandgap.

As far as the orbital hybridization is considered, we examine that the Au–d states are higher for doped systems as compared

with pure ones. Even for pure systems, the metal atoms at the interface tend to disturb the bonding of the nearest sulfur atoms with Mo leading to wave function overlaps. However, for the doped cases, both the dopant atoms, the interfacial gold atoms, and the decrease in the inter layer distance influence the Mo–S bonding, hence higher spikes are observed for all the two cases which covers the bandgap regime efficiently. This observation also leads to a better charge transport across the interface.

We resimulate all the MoS_2–Au interface structures using the Grimme's DFT-D2 [28] correction factor and the inter layer separations are found to be 2.8, 2.8, and 2.7 Å for pristine, 2-Nb and 4-Nb-doped geometries, respectively. While the nature of the band structure remains the same as Fig. 3, the respective p-type SBH gets modified to 1.356, 0.918, and 0.491 eV.

IV. Conclusion

Here, we present a comprehensive study to explore the contact nature of an interface formed of pure and Nb-doped MoS_2 supercell with Au for various doping concentrations. We first analyze the shifts in energy levels corresponding to pristine and doped structures and observe formation of degenerate p-type MoS_2 semiconductor. The electronic properties of an interface formed by supercell and Au contact are then studied to evaluate energy level shifts, SBHs, charge transfer and orbital hybridization. It is seen that there is a transition from n-type SBH for pure systems to p-type SBH for Nb-doped configurations. Therefore, we hereby conclude that p-type doping, which is successful in achieving p-type conduction in an inherent n-type MoS_2, facilitates in attaining efficient MoS_2–metal contacts as well.

Acknowledgment

The authors would like to thank Quantumwise support staffs for their useful discussions.

References

[1] B. Radisavljevic, A. Radenovic, J. Brivio, V. Giacometti, and A. Kis, "Single-layer MoS_2 transistors," *Nature Nanotechnol.*, vol. 6, no. 3, pp. 147–150, Mar. 2011.

[2] S. Kim *et al.*, "High-mobility and low-power thin-film transistors based on multilayer MoS_2 crystals," *Nature Commun.*, vol. 3, p. 1011, Aug. 2012.

[3] B. Radisavljevic, M. B. Whitwick, and A. Kis, "Integrated circuits and logic operations based on single-layer MoS_2," *ACS Nano*, vol. 5, no. 12, pp. 9934–9938, 2011.

[4] H. Wang *et al.*, "Integrated circuits based on bilayer MoS_2 transistors," *Nano Lett.*, vol. 12, no. 9, pp. 4674–4680, 2012.

[5] C.-H. Lee *et al.*, "Atomically thin p–n junctions with van der Waals heterointerfaces," *Nature Nanotechnol.*, vol. 9, pp. 676–681, Aug. 2014.

[6] D. Lembke and A. Kis, "Breakdown of high-performance monolayer MoS_2 transistors," *ACS Nano*, vol. 6, no. 11, pp. 10070–10075, 2012.

[7] K. Dolui, I. Rungger, C. Das Pemmaraju, and S. Sanvito, "Possible doping strategies for MoS_2 monolayers: An *ab initio* study," *Phys. Rev. B*, vol. 88, no. 7, Aug. 2013. [Online]. Available: http://link.aps.org/doi/10.1103/PhysRevB.88.075420

[8] J. Suh *et al.*, "Doping against the native propensity of MoS_2: Degenerate hole doping by cation substitution," *Nano Lett.*, vol. 14, no. 12, pp. 6976–6982, 2014.

[9] M. R. Laskar *et al.*, "p-type doping of MoS_2 thin films using Nb," *Appl. Phys. Lett.*, vol. 104, no. 9, p. 092104, 2014.

[10] F. L. Deepak *et al.*, "Fullerene-like (IF) $Nb_xMo_{1-x}S_2$ nanoparticles," *J. Amer. Chem. Soc.*, vol. 129, no. 41, pp. 12549–12562, 2007.

[11] P. Hohenberg and W. Kohn, "Inhomogeneous electron gas," *Phys. Rev.*, vol. 136, no. 3B, pp. B864–B871, Nov. 1964.

[12] W. Kohn and L. J. Sham, "Self-consistent equations including exchange and correlation effects," *Phys. Rev.*, vol. 140, no. 4A, pp. 1133–1138, Nov. 1965.

[13] J. P. Perdew, K. Burke, and M. Ernzerhof, "Generalized gradient approximation made simple," *Phys. Rev. Lett.*, vol. 77, no. 18, pp. 3865–3868, 1996.

[14] J. P. Perdew, K. Burke, and Y. Wang, "Generalized gradient approximation for the exchange-correlation hole of a many-electron system," *Phys. Rev. B*, vol. 54, p. 16533, 1996.

[15] *Atomistix ToolKit v.14.1 Quantumwise*. [Online]. Available: http://quantumwise.com/, accessed 2015.

[16] J. Kang, S. Tongay, J. Zhou, J. Li, and J. Wu, "Band offsets and heterostructures of two-dimensional semiconductors," *Appl. Phys. Lett.*, vol. 102, no. 1, p. 012111, 2013.

[17] C. Hartwigsen, S. Goedecker, and J. Hutter, "Relativistic separable dual-space Gaussian pseudopotentials from H to Rn," *Phys. Rev. B, Condens. Matter Mater. Phys.*, vol. 58, no. 7, pp. 3641–3662, Aug 1998. [Online]. Available: http://link.aps.org/doi/10.1103/PhysRevB.58.3641

[18] K. F. Mak, C. Lee, J. Hone, J. Shan, and T. F. Heinz, "Atomically thin MoS_2: A new direct-gap semiconductor," *Phys. Rev. Lett.*, vol. 105, no. 13, p. 136805, Sep. 2010. [Online]. Available: http://link.aps.org/doi/10.1103/PhysRevLett.105.136805

[19] H. J. Monkhorst and J. D. Pack, "Special points for Brillouin-zone integrations," *Phys. Rev. B*, vol. 13, no. 12, pp. 5188–5192, 1976.

[20] *LBFGS*. [Online]. Available: https://wiki.fysik.dtu.dk/ase/ase/optimize.htmlmodule-ase.optimize.lbfgs, accessed 2015.

[21] C. G. Van de Walle and J. Neugebauer, "First-principles calculations for defects and impurities: Applications to III-nitrides," *J. Appl. Phys.*, vol. 95, no. 8, pp. 3851–3879, 2004.

[22] W. Chen, E. J. Santos, W. Zhu, E. Kaxiras, and Z. Zhang, "Tuning the electronic and chemical properties of monolayer MoS_2 adsorbed on transition metal substrates," *Nano Lett.*, vol. 13, no. 2, pp. 509–514, 2013.

[23] J. Kang, W. Liu, D. Sarkar, D. Jena, and K. Banerjee, "Computational study of metal contacts to monolayer transition-metal dichalcogenide semiconductors," *Phys. Rev. X*, vol. 4, no. 3, p. 031005, 2014.

[24] G. Giovannetti, P. A. Khomyakov, G. Brocks, V. M. Karpan, J. van den Brink, and P. J. Kelly, "Doping graphene with metal contacts," *Phys. Rev. Lett.*, vol. 101, no. 2, pp. 026803-1–026803-4, 2008.

[25] C. Gong, G. Lee, B. Shan, E. M. Vogel, R. M. Wallace, and K. Cho, "First-principles study of metal–graphene interfaces," *J. Appl. Phys.*, vol. 108, no. 12, p. 123711, 2010.

[26] C. Gong, L. Colombo, R. M. Wallace, and K. Cho, "The unusual mechanism of partial Fermi level pinning at metal–MoS_2 interfaces," *Nano Lett.*, vol. 14, no. 4, pp. 1714–1720, 2014.

[27] *Quantumwise Reference Manual*. [Online]. Available: http://www.quantumwise.com/documents/manuals/latest/ReferenceManual/index.html/, accessed 2015.

[28] S. Grimme, "Semiempirical GGA-type density functional constructed with a long-range dispersion correction," *J. Comput. Chem.*, vol. 27, no. 15, pp. 1787–1799, 2006.

Anuja Chanana is currently pursuing the Ph.D. degree with the Nanoscale Device Research Laboratory, Department of Electronic Systems Engineering, Indian Institute of Science, Bangalore, India.

Santanu Mahapatra (M'08–SM'10) received the Ph.D. degree from the École Polytechnique Fédérale de Lausanne, Lausanne, Switzerland, in 2005.

He is currently an Associate Professor with the Indian Institute of Science, Bangalore, India.

Prof. Mahapatra was a recipient of the Ramanna Fellowship from the Department of Science and Technology, Government of India, for his contribution in compact modeling, in 2012.